Solid State Communications 150 (2010) 514–518

Contents lists available at ScienceDirect

Solid State Communications

journal homepage: www.elsevier.com/locate/ssc

Exploring thermoelectric effects and Wiedemann–Franz violation in magnetic nanostructures via micromachined thermal platforms

B.L. Zink [a,*], A.D. Avery [a], Rubina Sultan [a], D. Bassett [a], M.R. Pufall [b]

[a] Department of Physics & Astronomy, University of Denver, Denver, CO 80208-6900, United States

[b] National Institute of Standards and Technology, Magnetics Group, Boulder, CO 80305, United States

ARTICLE INFO

Article history:
Received 16 October 2009
Received in revised form
31 October 2009
Accepted 2 November 2009
by the Guest Editors
Available online 11 November 2009

Keywords:
A. Magnetic films and multilayers
A. Nanostructures
B. Heat conduction
B. Thermodynamic properties

ABSTRACT

We describe the development and use of micromachined thermal isolation structures to explore thermoelectric effects in magnetic thin films and nanostructures. These unique measurement techniques allow fundamental studies that will help enable a wide range of spin-caloritronic devices that take advantage of the coupling between heat and magnetic degrees of freedom for useful effects. The thermal platform is capable of measuring thermal conductivity, k, thermopower (Seebeck coefficient), α, and electrical conductivity, σ, all on the same thin film sample. This also allows direct comparison of the measured thermal conductivity of a magnetic thin film to the prediction of the Wiedemann–Franz law based on measured electrical conductivity. In addition to describing the fabrication of the platforms and the basic principles of their operation, we present example data on nickel and nickel–iron alloy thin films, and briefly consider the range of samples that can be measured with both current techniques and future thermal platforms optimized for nanoscale samples.

1. Introduction

The large volume of research on voltage-driven spin transport in magnetic materials and multilayers has led to a rich understanding of the process of polarization of conduction electrons by magnetic thin films and their resulting transport properties. However, much less is currently known about thermal effects in magnetic thin films, multilayers and nanostructures. This is because thermal measurements of very thin films and systems assembled from them are typically significantly more difficult than measuring electrical transport. The recent demonstration of the Spin Seebeck effect [1], and theoretical predictions of interesting effects including thermally-driven spin torques [2,3], has stimulated interest in thermoelectric phenomena in magnetic thin films and nanostructures that was previously most actively studied as a means to further understand transport in spin-valve structures [4–9]. Exploration of the consequences of coupling between phonons and spins in a wide range of materials and structures will help realize the promise of useful spin-caloritronic devices. This paper describes our work on direct measurements of thermal transport and thermopower in magnetic thin films made using micromachined silicon-nitride thermal isolation structures with sensitive integrated thermometers. These devices allow the careful control and measurement of in-plane thermal gradients required to make accurate thermal measurements even on structures approaching the nanoscale. These micromachined thermal platforms allow measurements of thermal, electronic, and thermoelectric transport on a single thin film sample, which also enables a direct examination of the Wiedemann–Franz law relating electrical and thermal conductivities in a material. Our techniques yield an experimental test of the validity of this relation of electrical and thermal conductivities in magnetic nanostructures. In the following sections we first describe the thermal isolation platforms and their use, then present example thermal conductivity and thermopower data for several ferromagnetic thin films. We then examine the Wiedemann–Franz predictions for these films, and finally consider the range of possible samples that can be measured with the existing thermal platform.

2. Measurement technique

The micromachined thermal isolation platform we use for these measurements is shown in Fig. 1. The thermal isolation structure

* Corresponding author.
E-mail address: barry.zink@du.edu (B.L. Zink).

0038-1098/$ – see front matter © 2009 Elsevier Ltd. All rights reserved.
doi:10.1016/j.ssc.2009.11.003

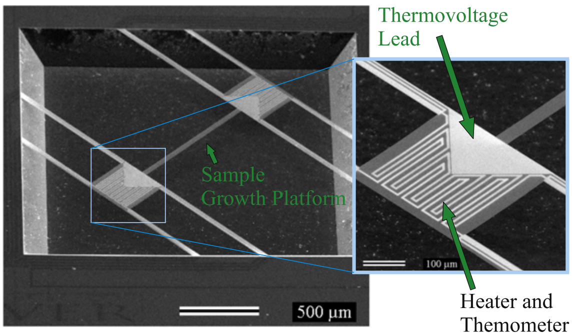

Fig. 1. Scanning electron micrographs of micromachined thermal platforms that allow measurements of thermal conductivity, thermopower, and the Lorenz number on thin film samples.

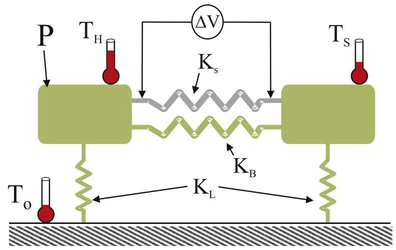

Fig. 2. A schematic showing the simple thermal model used to describe the micromachined thermal platforms. Before deposition of a sample, the only connection between the two islands is the background thermal conductance of the Si–N bridge. Adding a sample adds the thermal link K_S, modifying the thermal model. The thermovoltage generated by the temperature gradient is measured using the leads on either side of the bridge shown in Fig. 1.

is formed from a patterned 500 nm thick amorphous silicon-nitride (Si–N) layer. Metal heaters, thermometers, and leads are patterned on the top surface of this layer before the bulk Si is removed from beneath it using an anisotropic Si etch. This process releases the two islands and the narrow bridge between them, leaving only 8 narrow legs that connect the structure to the thermal bath at temperature T_o. The resulting thermal circuit is shown schematically in Fig. 2. Before a sample is deposited, the only thermal path from one island to the next is through the Si–N. This is the background thermal conductance of the platform and is represented by K_B. The conductance from the islands to the bath via the legs, K_L, is also shown.

Simple steady-state heat flow equations for this thermal circuit when Joule-heating power, P, is dissipated in one island's heater give expressions for the temperature of the two islands:

$$T_H = T_o + \frac{(K_L + K_B)P}{(2K_B + K_L)K_L} \tag{1}$$

$$T_S = T_o + \frac{(K_B)P}{(2K_B + K_L)K_L}. \tag{2}$$

To measure the background conductance, K_B, we regulate the temperature of the bath (the Si frame of the platform clamped to the Cu cold finger of a sample-in-vacuum cryostat) and measure the resistance of metal thermistors on the frame and each island for a range of heating powers. Calibration of the thermistors allows conversion of resistances to temperatures T_o, T_H and T_S, which are linear when plotted vs measured P as shown in Fig. 3. Linear fits to these plots allow determination of K_B (as well as K_L) according to Eqs. (1) and (2). Deposition of a sample on the bridge adds a contribution K_S to the conductance between islands. This new total conductance $K_S + K_B$ is measured in the same way, and the contribution of the sample determined by subtracting the previously measured background. The thermal conductivity of the

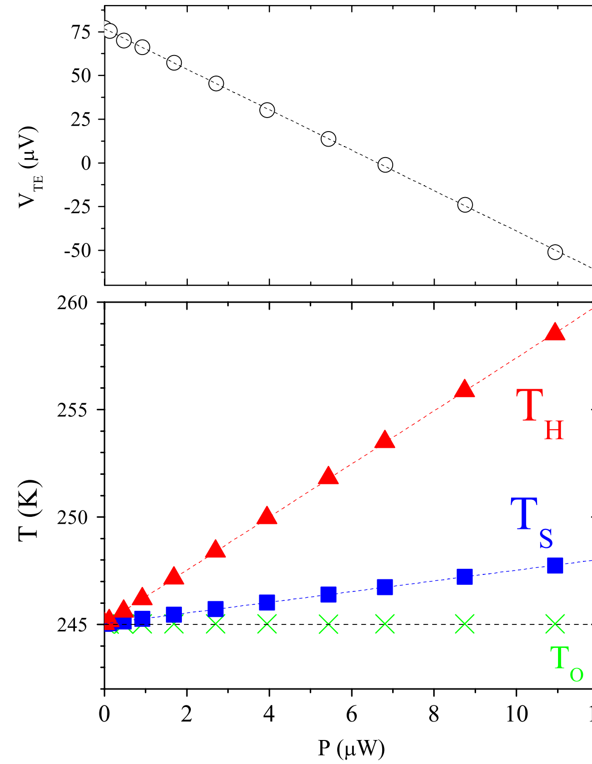

Fig. 3. The bottom panel shows the temperature of the platform's Si frame, T_o, the directly heated island, T_H, and the island heated by heat flow down K_B, T_S. Linear fits of T_H and T_S vs P as shown are used to determine values of K_B and K_L. The top panel shows the thermovoltage generated across the film as power is applied. The slope of the line fit to this data gives the thermopower or Seebeck coefficient, α.

sample is determined from K_S and sample geometry, $k = K_S l/wt$, where l and w are the length and width of the bridge and t is the thickness of the sample film. The addition of electrical leads that contact the sample on either side of the bridge allow measurement of the thermovoltage at each power as shown in Fig. 3, which allows determination of the Seebeck coefficient by determining the slope of ΔV vs. ΔT. Further details of the use and fabrication of the thermal platforms is discussed elsewhere [10].

For thermoelectric power measurements, several 75 nm thick permalloy (Ni–Fe) films (approximate composition 80% Ni, 15% Fe, and 5% Mo) were deposited on the thermal platforms via e-beam evaporation through micromachined shadow masks. Growth rates from 0.4–1.3 nm/s were used, after reaching base pressures in a UHV deposition chamber of better than 1×10^{-8} Torr. Pressure during growth increased less than a factor of 10 for all films. These permalloy films are compared to an elemental nickel film that was sputtered on the platform and patterned via photoresist liftoff before platform release. In order to provide the most accurate k measurements to test the Wiedemann–Franz Law, one Ni–Fe film was deposited on the Si–N bridge after the background thermal conductance was previously measured. This eliminates any additional uncertainty in the background conductance, which can vary by several percent even among platforms fabricated on the same wafer [10]. This can be important for low thermal conductivity samples such as the Ni–Fe alloy.

3. Results and discussion

Fig. 4 compares the total thermal conductance for two different samples to that of the Si–N background. Sputtering a 50 nm thick nickel film on the 500 nm Si–N bridge adds a very significant thermal conductance, more than doubling the bridge contribution, K_B, near room temperature. This is expected since highly conductive metallic films typically have very large thermal

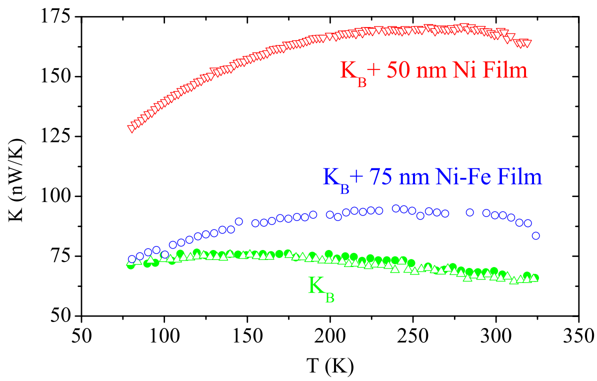

Fig. 4. Thermal Conductance of the Si–N bridge, K_B, compared to the total conductance after a 75 nm thick Ni–Fe film, and a 50 nm Ni film are deposited. A thinner layer of Ni adds a much larger thermal conductance than the Ni–Fe.

conductivities compared to the disordered insulating Si–N. It is obvious, however, that the 75 nm Ni–Fe film has a much lower thermal conductivity since its contribution to the total conductance is much lower. One also notes that the temperature dependence of k for Si–N (obvious here in the shape of K_B and of course in $k_{\text{Si–N}}$ shown in Fig. 5(b)) departs somewhat from the typical expectation for an amorphous insulator [11], which is a gradual but increasing slope at these temperatures. We have observed this behavior in dozens of separate thermal platforms fabricated on several different wafers. One interpretation is that at these temperatures the Si–N is still in the "plateau" regime seen in many amorphous insulators. As discussed further elsewhere [10], it is also possible that the Si–N is not purely amorphous. Though this is an interesting phenomena that we continue to study, the Si–N bridge serves its intended purpose for this experiment, in providing a suitably low background conductance.

The low conductivity of the Ni–Fe alloy is expected and verified by the electrical resistivity data shown in Fig. 5(a). This plot compares results for the Ni–Fe film to that of the elemental Ni film. The Ni film's values are typical for reasonably pure metal films, while the disorder in the alloy film drives ρ much higher, though the values remain in the range typically observed for permalloy films. This trend is also seen in the k data shown in Fig. 5(b), where data for the films are compared to bulk Ni, two bulk alloys, and the predominantly amorphous Si–N that forms the sample platform.

One distinct advantage to our technique for measuring transport in thin films and nanostructures is the ability to measure electrical and thermal transport on the same sample. This allows examination of the Wiedemann–Franz law with no additional uncertainty from sample geometry or compositional variations between films. The Wiedemann–Franz law can be derived from simple free-electron theory and, when obeyed, is a strong indication of relatively simple Fermi liquid behavior and that the same scattering mechanisms dominate both thermal and electrical processes in a sample. This ratio of the electron thermal conductivity to the electrical conductivity is a simple expression:

$$\frac{k_e}{\sigma} = LT, \tag{3}$$

where L is the constant Lorenz number that for many metals is near the Sommerfeld value of $L_o = 2.44 \times 10^{-8}$ WΩ/K^2. When thermal and electrical transport are measured on the same sample, determination of L requires only the temperature and the extensive, directly measured quantities K_S and R:

$$L = \frac{K_S R}{T}. \tag{4}$$

The Lorenz number determined this way is plotted vs. T in Fig. 6 for Ni and Ni–Fe films compared to bulk Ni and a suspended Ni

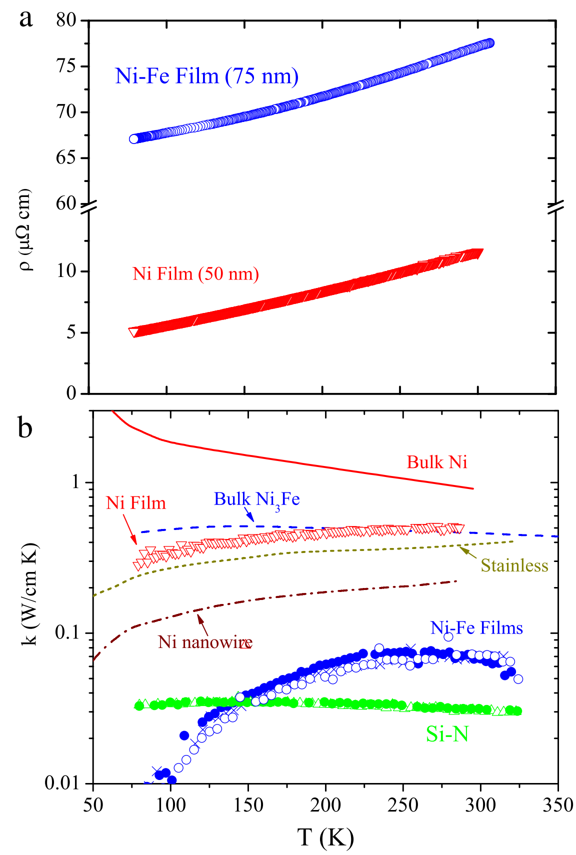

Fig. 5. (a) Electrical resistivity, ρ vs. T measured for films on thermal platforms. The inherently disordered Ni–Fe alloy film has much higher ρ than the elemental Ni film. (b) Thermal conductivity, k vs. T for Ni and Ni–Fe films compared to bulk Ni [13], bulk Ni_3Fe [14], stainless steel [15], and a Ni nanowire [12]. Values for the Si–N that forms the bridge are also shown.

nanowire measured via different techniques by another group [12]. Note that we use the total sample conductance in Eq. (4) (or the total thermal conductivity in Eq. (3)) which can include non-electronic contributions such as phonon thermal conductivity in the numerator of L, and cause an apparently high value of L. A phonon contribution that is comparable to the electron k is the explanation offered by Ou, et al. for the constant positive offset in L seen in their highly disordered Ni nanowire.

In bulk metals a dip in L as temperature drops below the Debye temperature and a subsequent return to values near L_o in the residual resistivity regime is commonly observed and well understood. Thermal and electrical transport are governed by the same scattering processes leading to values near L_o when large-angle scattering of electrons from static disorder (low T) or from energetic phonons (high T) dominates. The dip occurs where small-angle scattering of electrons from phonons of lower energy affects thermal conduction more strongly, driving k_e down with respect to σ. The bulk Ni values shown follow this trend, though with L somewhat lower than L_o and on the lower range of values seen for typical metals. Values for the Ni film match the bulk behavior reasonably well at high temperatures, though the dip in L is not apparent at the lowest temperatures currently available. In fact L for this 50 nm thick sputtered nickel film seems remarkably temperature independent with a value near 1.9×10^{-8} WΩ/K^2. The origin of these behaviors is not immediately apparent. Examination of Eq. (4) suggests the possibility that either the thermal conductance K_S or the resistance R could be underestimated, which is difficult to explain with systematic effects that could complicate our experiment such as contact resistance between the film and the two electrical

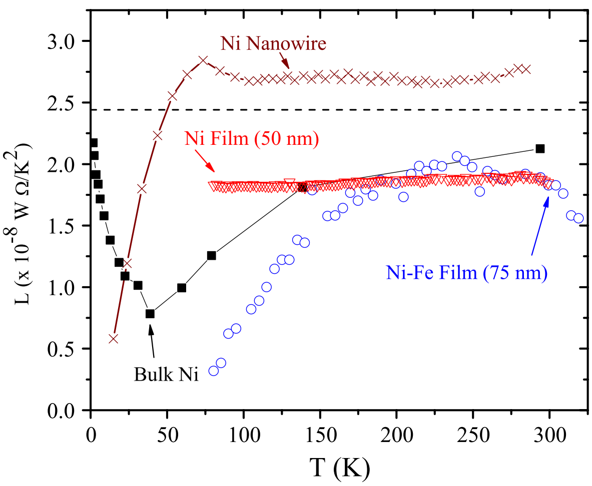

Fig. 6. Experimentally determined values for the Lorenz number, L vs. T for two ferromagnetic thin films compared to bulk Ni [16], a Ni nanowire [12], and the Sommerfeld value, L_o.

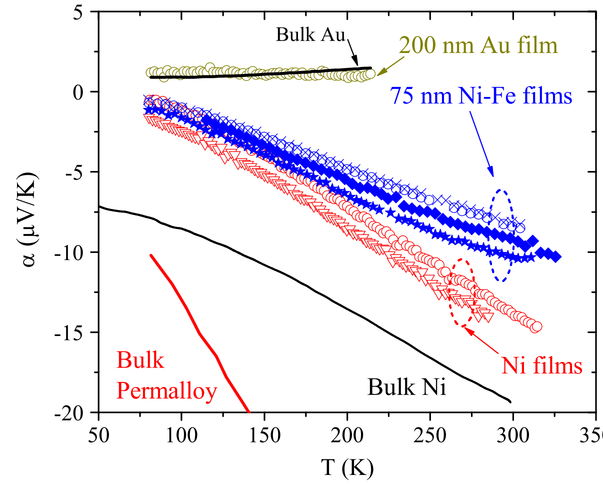

Fig. 7. Thermopower of several Ni and Ni–Fe alloy thin films compared to bulk Ni [16], bulk permalloy [19], and a Ni nanowire [17].

leads. It is possible that this result suggests that some additional scattering mechanism exists in this film that affects thermal transport more strongly than electrical transport. Another possible explanation is that either the phonon or the magnon spectrum could be significantly modified in the thin film, which could allow large wavevector excitations required for the large-angle scattering that normally dominates at high T to remain active at lower temperatures. This would effectively extend the range of agreement with the Wiedemann–Franz law to lower T as seen in the Ni film.

Between 300 and 150 K the measured values of L for the permalloy film are in general agreement with the Ni film, with a room temperature value of the Lorenz number of $\sim 1.9 \times 10^{-8}$ WΩ/K^2. This is an important result since values of the thermal conductivity of permalloy films required to model thermal effects in various magnetic devices could be significantly overestimated by using the Wiedemann–Franz law with the typical value of L_o. Interestingly, the Ni–Fe alloy film does show a reduction of L as temperature drops. If the Ni film's magnon and/or vibrational spectrum is indeed softened, the more typical temperature dependence of L in the Ni–Fe film could suggest that the alloy remains relatively stiffer, preventing thermal activation of large wavevector excitations at these temperatures. In any case it is clear that the issue of the temperature dependence of L requires further study in a range of metals in thin film form.

The measured thermopower (or Seebeck coefficient) of several ferromagnetic thin films is compared to bulk values from the literature in Fig. 7. Two sputtered Ni films (of thickness 50 nm and 100 nm) show similar thermopower from 80–300 K, with a temperature dependence comparable to that seen in bulk Ni at these temperatures, but with an apparent approximately constant offset. This offset is similar to the behavior seen in the thermopower of a Ni nanowire measured by another technique [17], which again has a similar slope with temperature but a constant offset. This suggests that the Ni films show a similar diffusive thermopower modified by strong disorder as seen in the nanowire. Three different 75 nm Ni–Fe alloy films all show similar thermopower as a function of temperature. Here the behavior is dramatically different than seen in bulk permalloy, with much smaller negative values and a weaker temperature dependence. The origin of this discrepancy is an area for future study. Also note that one Ni–Fe film was measured both in zero applied magnetic field and with a 100 Oe field applied along the direction of the bridge. There is no measurable difference between the unmagnetized and fully magnetized states that can be determined from our current data. The same lack of field dependence occurred in thermal transport, and might seem odd since the magnetic field dependence of the electrical transport is well known in permalloy films. However, even when samples are grown in field in order to align the easy axis of magnetization optimally with respect to the current direction and thus maximize the anisotropic magnetoresistance [18], the maximum change in field is only a few percent. Magnetoresistance measurements on our films in fact indicate even smaller changes with the field oriented as applied, and our thermal measurements are currently not sensitive enough to detect these tiny field dependent changes. Magnetic nanostructures such as AF–F coupled multilayers show much larger changes in transport with applied field and will be interesting to study with our techniques.

Finally, we consider the question of what range of thin film or nanostructured samples can be effectively measured using our current thermal isolation platforms. This is largely determined by the error that arises from subtracting the background thermal conductance. In Fig. 8 we use the measured background conductance of the Si–N bridge, K_B to estimate the relative error in measured thermal conductance of both the thin ferromagnetic films discussed above, and of a parallel array of small wires that could be patterned on the thermal platforms via e-beam lithography. The dashed lines are estimated contributions to K_S from arrays of nanowires of resistivity similar to the Ni film, calculated by simple scaling of the thermal conductivity of sputtered films in the bulk limit. Colored solid lines indicate expected relative error on K_s measurements, assuming 0.5% relative error on measurements of K_b both before and after the nanowire array is added. This estimate suggests that highly accurate measurements of arrays of a modest number of wires of width well below 100 nm are realistic. Measurements of this type would be an important test of Wiedemann–Franz behavior in such nanowire systems, and could also be used to test field dependence of thermal effects in these tiny structures. Note also that these predictions are all based on our existing micromachined thermal platform; we are in the early stages of designing a nanomachined bridge structure to be fabricated using e-beam lithography that will be significantly more sensitive.

4. Conclusion and future outlook

In summary, we have overviewed our recently developed techniques for measuring thermal transport and thermopower in thin films and nanostructures and presented measurements of the thermal conductivity, thermopower, and measured Lorenz number as a function of temperature. The results indicate that permalloy thin films have a low thermal conductivity, and roughly follow the

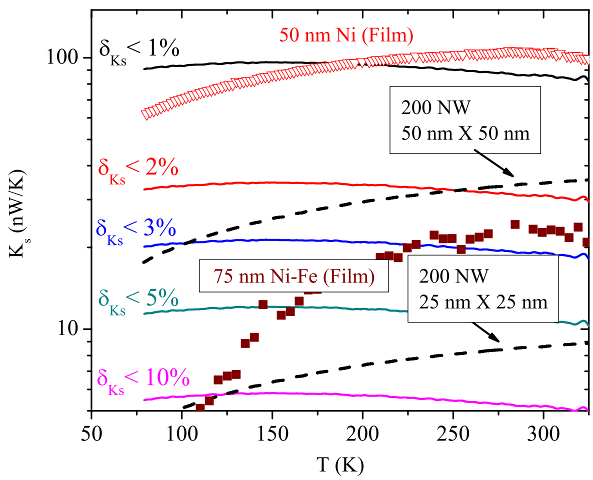

Fig. 8. Predicted measurement accuracy for thin films and arrays formed from metal nanowires using the micromachined thermal platforms. A platform optimized for nanolithographic structures will allow much more sensitive measurements.

behavior predicted by the Wiedemann–Franz law but with a value near room temperature significantly less than the Sommerfeld value and the values seen in bulk nickel. Our future work will focus on extending these techniques to lower temperatures and smaller samples, as well as adding capability to measure spin currents that will allow exploration of phenomena such as the Spin Seebeck effect for a wide range of materials systems.

Acknowledgements

The authors would like to acknowledge the support of the Nanoelectronics Research Institute and the National Science Foundation (DMR-0847796). We also thank J. Stoke for assistance designing and constructing the UHV system, J. Beall and G. Hilton for numerous conversations on and contributions to device fabrication, and C. Leighton for valuable discussions of UHV growth techniques.

References

[1] K. Uchida, S. Takahashi, K. Harii, J. Ieda, W. Koshibae, K. Ando, S. Maekawa, E. Saitoh, Nature 455 (2008) 778.
[2] M. Hatami, G.E.W. Bauer, Q. Zhang, P.J. Kelly, Physical Review B 79 (2009) 174426.
[3] M. Hatami, G.E.W. Bauer, Q. Zhang, P.J. Kelly, Physical Review Letters 99 (2007) 066603.
[4] L. Gravier, S. Serrano-Guisan, F. Reuse, J.-P. Ansermet, Physical Review B (Condensed Matter and Materials Physics) 73 (2006) 024419.
[5] L. Gravier, S. Serrano-Guisan, F. Reuse, J.-P. Ansermet, Physical Review B (Condensed Matter and Materials Physics) 73 (2006) 052410.
[6] A. Fukushima, H. Kubota, A. Yamamoto, Y. Suzuki, S. Yuasa, Journal of Applied Physics 99 (2006) 08H706.
[7] E.Y. Tsymbal, D.G. Pettifor, J. Shi, M.B. Salamon, Physical Review B 59 (1999) 8371.
[8] J. Shi, S.S.P. Parkin, L. Xing, M.B. Salamon, Journal of Magnetism and Magnetic Materials 125 (1993) L251.
[9] L. Piraux, A. Fert, P.A. Schroeder, R. Loloee, P. Etienne, Journal of Magnetism and Magnetic Materials 110 (1992) L247.
[10] R. Sultan, A.D. Avery, G. Stiehl, B.L. Zink, Journal of Applied Physics 105 (2009) 043501.
[11] R.C. Zeller, R.O. Pohl, Physical Review B 4 (1971) 2029.
[12] M.N. Ou, T.J. Yang, S.R. Harutyunyan, Y.Y. Chen, C.D. Chen, S.J. Lai, Applied Physics Letters 92 (2008) 063101.
[13] T. Farrell, D. Greig, Journal of Physics C (Solid State Physics) 2 (1969) 1465.
[14] J.P. Moore, T.G. Kollie, R.S. Graves, D.L. McElroy, Journal of Applied Physics 42 (1971) 3114. ISSN:0021-8979.
[15] G.E. Childs, L.J. Ericks, R.L. Powell, NBS Monograph Number M131, 1973.
[16] F.J. Blatt, D.J. Flood, V. Rowe, P.A. Schroeder, J.E. Cox, Physical Review Letters 18 (1967) 395.
[17] E. Shapira, A. Tsukernik, Y. Selzer, Nanotechnology 18 (2007) 485703.
[18] T.R. McGuire, R.I. Potter, IEEE Transactions on Magnetics MAG-11 (1975) 1018.
[19] C.Y. Ho, R.H. Bogaard, T.C. Chi, T.N. Havill, H.M. James, Thermochimica Acta 218 (1993) 29.